



A highly efficient NiCo₂O₄ decorated g-C₃N₄ nanocomposite for screen-printed carbon electrode based electrochemical sensing and adsorptive removal of fast green dye

Ankit Kumar Singh¹ · Shreanshi Agrahari¹ · Ravindra Kumar Gautam¹ · Ida Tiwari¹

Received: 12 July 2023 / Accepted: 6 October 2023

© The Author(s), under exclusive licence to Springer-Verlag GmbH Germany, part of Springer Nature 2023

Abstract

Herein, we demonstrate the preparation and application of NiCo₂O₄ decorated over a g-C₃N₄-based novel nanocomposite (NiCo₂O₄@g-C₃N₄). The prepared material was well characterized through several physicochemical techniques, including FT-IR, XRD, SEM, and TEM. The electrochemical characterizations via electrochemical impedance spectroscopy show the low electron transfer resistance of NiCo₂O₄@g-C₃N₄ owing to the successful incorporation of NiCo₂O₄ nanoparticles on the sheets of g-C₃N₄. NiCo₂O₄@g-C₃N₄ nanocomposite was employed in the fabrication of a screen-printed carbon electrode-based innovative electrochemical sensing platform and the adsorptive removal of a food dye, *i.e.*, fast green FCF dye (FGD). The electrochemical oxidation of FGD at the developed NiCo₂O₄@g-C₃N₄ nanocomposite modified screen-printed carbon electrode (NiCo₂O₄@g-C₃N₄/SPCE) was observed at an oxidation potential of 0.65 V. A wide dual calibration range for electrochemical determination of FGD was successfully established at the prepared sensing platform, showing an excellent LOD of 0.13 μM and sensitivity of 0.6912 μA·μM⁻¹·cm⁻² through differential pulse voltammetry. Further, adsorbent dose, pH, contact time, and temperature were optimized to study the adsorption phenomena. The adsorption thermodynamics, isotherm, and kinetics were also investigated for efficient removal of FGD at NiCo₂O₄@g-C₃N₄-based adsorbents. The adsorption phenomenon of FGD on NiCo₂O₄@g-C₃N₄ was best fitted ($R^2=0.99$) with the Langmuir and Henry model, and the corresponding value of Langmuir adsorption efficiency (q_m) was 3.72 mg/g for the removal of FGD. The reaction kinetics for adsorption phenomenon were observed to be pseudo-second order. The sensitive analysis of FGD in a real sample was also studied.

Keywords Adsorption · Electrochemical sensing · Fast green dye · Graphitic carbon nitride · Screen-printed electrodes

Responsible Editor: Weiming Zhang

Highlights

- NiCo₂O₄ decorated over g-C₃N₄(NiCo₂O₄@g-C₃N₄) nanocomposite was prepared.
- Dual role of NiCo₂O₄@g-C₃N₄ nanocomposite as a sensing material and as an adsorbent was studied.
- A novel screen-printed carbon electrode-based sensor for fast green dye (FGD) was fabricated.
- A wide calibration range (0.2-800 μM) for sensing of FGD was established.
- High percentage (95.38 %) removal of FGD was observed at NiCo₂O₄@g-C₃N₄.

✉ Ida Tiwari
idatiwari_2001@rediffmail.com

Ankit Kumar Singh
anksingh325@gmail.com

Introduction

Several synthetic dyes are introduced into the food supplements to make them more visually attractive to buyers (Shah 2020). Fast Green FCF dye (FGD; *c.f.* Fig. S1), an acidic dye, is commonly employed as a food colouring reagent and is also called ‘food dye’ (Abdi and Nasiri 2018). This dye is used to stain proteins in electrophoresis and to colour a variety of tinned foods, including green peas, vegetables, fish, and desserts (Abdi and Nasiri 2018)(Ahmed and Hossain

¹ Department of Chemistry (Centre of Advanced Study), Institute of Science, Banaras Hindu University, Varanasi 221005, India

2021). Fast Green FCF is the most commonly used food colours despite being banned in certain developed nations. FGD is extremely toxic and allergic, affecting the respiratory system and causing irritation to the skin, eyes, and nasal passages (Shetti and Nayak 2016). It also inhibits the secretion of neurotransmitters (Shah 2020). Despite the known hazards, food manufacturers are continuously using FGD because it is considerably cheaper than natural dyes. Thus, there is an important need to develop sensitive and highly efficient analytical methods for the detection and effective removal of FGD present in wastewater, both for the sake of public health safety and quality control.

In this context, several analytical techniques, including high-performance liquid chromatography, gas chromatography-mass spectrometry, and Raman spectroscopy, are widely used in the quantitative measurement of toxic dyes (Shah 2020). However, due to their high cost and complicated procedures (Shah 2020)(Beitollahi et al. 2022)(Christ-Ribeiro et al. 2022), the stakeholders have been forced to invest in the fabrication of a sensitive and selective electrochemical sensor for the analysis of very low concentrations of FGD. Moreover, a miniaturised and simple electrochemical sensor based on a screen-printed carbon electrode (SPCE) might be an ideal choice (Beitollahi et al. 2022) for onsite monitoring of FGD in wastewater. Further, several methods such as solvent extraction, chemical precipitation, biodegradation, membrane separation, ion-exchange, and adsorption are reported for effective removal of toxic dyes from wastewater (Singh et al. 2022b)(Yahya et al. 2022). However, adsorption is a highly successful technique to remove dyes owing to its high efficiency, low cost, excellent recovery, short time, and ease of use (Gautam et al. 2021)(Verma et al. 2022).

There are only a few publications available in the literature for electrochemical sensing of FGD (Shah 2020)(Shetti and Nayak 2016) as well as for adsorption of FGD from wastewater (Abdi and Nasiri 2018)(Tahir et al. 2008) but none of them report the sensing and adsorptive removal of FGD on the same nanocomposite. Also, the reported FGD sensors were based on the modification of a glassy carbon electrode (Shah 2020)(Shetti and Nayak 2016). Thus, it is an urgent requirement to prepare a bifunctional nanocomposite that might act as an adsorbent for the removal of FGD as well as an SPCE modifying material for the sensing of FGD.

Recently, mixed metal oxide-based nanomaterials have demonstrated excellent electrical conductivity and extensive surface areas; thus, they have been applied as electrode-modifying materials for electrochemical sensing applications (Fazio et al. 2021)(Rahman et al. 2019). Also, they exhibit inherent surface reactivities and environmental friendly nature for the adsorptive removal of toxic dyes (Arora et al. 2016)(Lashanizadegan et al. 2019). Especially, inverse spinel structured nickel cobaltite (NiCo_2O_4) has shown wide applications in the fields of sensors, fuel cells, photovoltaic

cells, photocatalysis, water splitting, and adsorption (Sudha et al. 2020)(Wang et al. 2013)(Anu Prathap and Srivastava 2013). In addition, NiCo_2O_4 nanoparticles exhibit higher catalytic activity towards electrochemical detection of analytes (Yuan et al. 2012). The electrocatalytic performance and conductivity of NiCo_2O_4 nanoparticles for the fabrication of FGD sensors, as well as their stability and high active surface area for adsorption of FGD, can be further improved by modifying them with polymers or carbon-based nanomaterials. In this work, NiCo_2O_4 nanoparticles are integrated over graphitic carbon nitride ($\text{g-C}_3\text{N}_4$) sheets ($\text{NiCo}_2\text{O}_4@ \text{g-C}_3\text{N}_4$) to improve the electrochemical as well as adsorption properties.

The $\text{g-C}_3\text{N}_4$ is a metal-free polymeric semiconductor having planar nanosheets where carbon and nitrogen atoms are sp^2 bonded to each other (Paul et al. 2019b)(Paul et al. 2023) and is greatly attracted because of its physical, chemical, and mechanical properties (Singh et al. 2022c)(Sharma et al. 2022)(Paul et al. 2019a). The facile synthesis and purely organic nature of $\text{g-C}_3\text{N}_4$ represent its key strengths (Paul et al. 2020b). It is highly stable, non-toxic, inert, cost-effective, and provides large active sites (Singh et al. 2021). These properties significantly improve the electrochemical as well as adsorption properties of the embedded mixed metal oxide nanoparticles. There are several works reporting the use of $\text{g-C}_3\text{N}_4$ -based materials in electrochemical sensing (Singh et al. 2022c)(Singh et al. 2022a) and dyes removal (Dahiya et al. 2023a)(Dahiya et al. 2023b)(Rao et al. 2023)(Paul et al. 2022a)(Shoran et al. 2023)(Shoran et al. 2022)(Paul et al. 2020a)(Paul et al. 2022b). Also, the nanomaterials show antimicrobial activities and thus represent environmental sustainability (Panchal et al. 2022)(Panchal et al. 2021)(Panchal et al. 2020)(Panchal et al. 2019b)(Panchal et al. 2019a).

In the present work, the successfully prepared $\text{NiCo}_2\text{O}_4@ \text{g-C}_3\text{N}_4$ nanocomposite has been used for sensitive electrochemical determination and adsorptive removal of FGD to treat contaminated water. The synthesized nanocomposite was incorporated on the surface of SPCE to fabricate a highly sensitive electrochemical FGD sensor. The exceptional electrochemical properties and conducting behavior of $\text{NiCo}_2\text{O}_4@ \text{g-C}_3\text{N}_4/\text{SPCE}$, along with its highly effective surface area, offer an excellent platform for the oxidation of FGD with a significant decrease in overpotential. The surface provided by the developed $\text{NiCo}_2\text{O}_4@ \text{g-C}_3\text{N}_4$ nanocomposite was able to adsorb a large amount of FGD. Thus, the produced $\text{NiCo}_2\text{O}_4@ \text{g-C}_3\text{N}_4$ nanocomposite provided an exceptional adsorption capacity for the removal of FGD from the wastewater. Notably, as far as we are able to know, this is the maiden report where $\text{NiCo}_2\text{O}_4@ \text{g-C}_3\text{N}_4$ nanocomposite was employed as a bifunctional material as an adsorbent as well as in the development of an SPCE-based sensing platform for FGD. Real wastewater samples

were also analyzed for the quantitative determination of FGD using the developed sensor.

Experimental section

Reagents and chemicals

Fast Green FCF (molecular formula, $C_{37}H_{34}N_2O_{10}S_3Na_2$; molecular weight, 808.85 g/mol) was purchased from SRL, India. Nickel nitrate hexahydrate ($Ni(NO_3)_2 \cdot 6H_2O$) and cobalt nitrate hexahydrate ($Co(NO_3)_2 \cdot 6H_2O$) were acquired from Sigma-Aldrich, USA, and Alfa Aesar, England, respectively. Urea (NH_2CONH_2) was provided by SRL, India. NaH_2PO_4 and Na_2HPO_4 were procured from HiMedia, Mumbai, India and Merck, Mumbai, India, respectively. Screen-printed carbon electrodes (DRP-110) were purchased from Metrohm DropSens India Private Limited, Chennai, India. All the solutions were prepared in triple-distilled water.

Instruments

The Fourier transform infrared (FT-IR) spectra of the prepared nanomaterials were analysed on a Perkin Elmer (Spectrum Two) Fourier transform infrared spectrophotometer. Powder X-ray diffraction (XRD) was measured at λ value of 1.5418 Å on the D8 Advance/Discover Bruker Germany, Diffractometer. Zeiss Evo 18 Research, coupled with energy-dispersive X-ray (EDX) spectroscopy, was used for scanning electron microscopy (SEM) and elemental analysis. Transmission electron microscopy (TEM) was performed on a TECNAI 20 G² FEI microscope. Thermogravimetric analysis (TGA) and UV–visible (UV–vis) analysis were carried out on Perkin Elmer (STA 6000) and Hitachi U3900 spectrophotometer, respectively. The electrochemical analysis was done on a Metrohm Autolab, PGSTAT302N with Nova 2.1.4 software connected to a three-electrode system. The SPCE (DRP-110) was used as a three-electrode cell with carbon as the working (diameter = 4 mm) and counter electrode and silver as the pseudo-reference electrode printed in carbon ink.

Methodology

Synthesis of g-C₃N₄

The preparation of g-C₃N₄ was performed as stated in our previously published works (Singh et al. 2021, 2022a). Typically, 15 g of urea was heated directly in a muffle furnace at 550 °C for its thermal decomposition to produce g-C₃N₄. Urea powder was kept in a silica crucible, and heating was provided at a rate of 6 °C/minute for 4 h. After complete decomposition, it was cooled to room temperature to get

a white colored powder. It was collected and cleaned with ethanol to remove unwanted impurities. The obtained powder was dried at 100 °C under vacuum conditions and collected for further use.

Synthesis of nickel cobaltite

NiCo₂O₄ nanoparticles were synthesized by a simple coprecipitation method as reported in the literature with little modifications (Kaur et al. 2022a). Typically, 2.48 g of $Co(NO_3)_2 \cdot 6H_2O$ was dissolved in 20 ml of water, and 0.9891 g of $Ni(NO_3)_2 \cdot 6H_2O$ was dissolved in 15 ml of water. The aqueous solution of nickel nitrate was slowly added to the cobalt nitrate solution with continuous stirring at 1000 rpm. Even after complete mixing of both solutions, the stirring was continued for 1 h, and then the 6 M KOH solution was added drop by drop, resulting in the formation of nickel–cobalt hydroxide precipitates. The obtained precipitates were filtered, washed with triple-distilled water and ethanol, and then dried in a vacuum oven. The completely dried product was calcined at 500 °C in a furnace for 4 h to get NiCo₂O₄ nanoparticles.

Preparation of NiCo₂O₄@g-C₃N₄ nanocomposite

The NiCo₂O₄@g-C₃N₄ nanocomposite was synthesized by mixing equal amounts of g-C₃N₄ and NiCo₂O₄ through ultrasonication, followed by stirring under reflux conditions. Initially, 50 mg g-C₃N₄ and 50 mg NiCo₂O₄ were separately well dispersed in methanol for 1 h through ultrasonication. The prepared dispersions were mixed together and further ultrasonicated for 1 h. The clearly dispersed mixture was allowed to stir and refluxed at 80 °C for 24 h. The obtained product was collected by centrifugation and thoroughly washed. Lastly, the synthesized nanocomposite was completely dried at 80 °C and kept in an air-tight bottle.

Determination of pH_{zpc}

The surface charges of the adsorbent that affect the decolorization of dye depend on the pH of the dye solution, and thus, it is required to calculate the pH at zero-point charge (pH_{zpc}). The pH_{zpc} of NiCo₂O₄@g-C₃N₄ nanocomposite was determined by a method reported in the literature (Singh et al. 2022b)(Khan and Sarwar 2007). For this, a 0.1 N KCl solution was prepared, and its 50 mL volume was taken in different flasks. The initial pH (pH_{initial}) of KCl solutions taken in different flasks was maintained between 2 and 12 using 0.1 N HCl or 0.1 N NaOH. Then, an adsorbent dose of 25 mg was added and stirred for 24 h at room temperature. The final pH (pH_{final}) of the solution was determined, and a graph was plotted between the difference of the final and initial pH values versus the initial pH, as represented in Fig. S2.

The pH where $\text{pH}_{\text{final}} - \text{pH}_{\text{initial}} = 0$ was considered pH_{zpc} . The value of pH_{zpc} for $\text{NiCo}_2\text{O}_4@ \text{g-C}_3\text{N}_4$ nanocomposite was determined to be 6.7.

Preparation of modified electrodes

For the fabrication of nanocomposite modified SPCE, 6 μL aqueous dispersion (1 mg/1 mL) of the prepared $\text{NiCo}_2\text{O}_4@ \text{g-C}_3\text{N}_4$ nanocomposite was dropped on the surface of SPCE. Then, it was dried at room temperature under ambient laboratory conditions to prepare $\text{NiCo}_2\text{O}_4@ \text{g-C}_3\text{N}_4/ \text{SPCE}$. For the comparison study, $\text{g-C}_3\text{N}_4/ \text{SPCE}$, $\text{NiCo}_2\text{O}_4/ \text{SPCE}$, and $\text{NiCo}_2\text{O}_4@ \text{g-C}_3\text{N}_4/ \text{GCE}$ were also prepared in a similar manner. Prior to modification, GCE was cleaned with 0.05 μm alumina powder followed by ultrasonication in triple distilled water and acetone to get a mirror like shining surface.

Electrochemical measurements

The preliminary study of the electrochemical behavior of FGD was examined through DPV using $\text{NiCo}_2\text{O}_4@ \text{g-C}_3\text{N}_4/ \text{SPCE}$ as a working electrode. The DPV was performed by taking 10 ml of 0.1 M PBS (pH 7.0) in an electrochemical cell as the supporting electrolyte. The potential for DPV studies was maintained in the range of 0.2 to 0.9 V until a steady voltammogram was attained. An appropriate amount of FGD solution of known concentration was added to the electrolyte present in the electrochemical cell, and it was mixed at 250 rpm using the magnetic stirrer. Again, DPV was measured in the same potential range. Further, an EIS study was also performed at $\text{NiCo}_2\text{O}_4@ \text{g-C}_3\text{N}_4/ \text{SPCE}$ in the presence of FGD to check the interfacial properties of the fabricated electrode. Triplicate measurements of each analysis were performed under ambient laboratory conditions.

Adsorption method

The adsorption efficiency of the synthesized $\text{NiCo}_2\text{O}_4@ \text{g-C}_3\text{N}_4$ was evaluated by examining the removal of FGD from water. The stock solution of FGD (1000 mg/L) was prepared in triple distilled water. Further, standard solutions of the required concentrations (1, 2, 3, 4, 5, and 6 mg/L) of dye were prepared from the stock solution by diluting it in triple-distilled water. Various parameters, including adsorbent dose, pH, contact time, and temperature, were optimized to achieve maximum removal of FGD. The adsorption studies were performed in batch experiments by adding an optimized dose (50 mg) of $\text{NiCo}_2\text{O}_4@ \text{g-C}_3\text{N}_4$ to 25 mL of 10 mg/L FGD dye as a fixed volume in conical flasks. The mixture was agitated on a magnetic stirrer for a fixed time, and then the adsorbent was removed from the solution through ultracentrifugation. The residual amount of

dye in the solution was determined by knowing the absorbance values before and after adsorption at a wavelength of 625 nm (λ_{max} of FGD) using a UV–visible spectrophotometer. The equilibrium adsorption capacity (q_e , mg/g) and the percentage removal of dye ($R\%$) were estimated using Eqs. (1) and (2), respectively (Muinde et al. 2020).

$$q_e = \frac{(C_o - C_e)V}{W} \quad (1)$$

$$R\% = \frac{(C_o - C_e)}{C_o} \times 100 \quad (2)$$

Here, C_o and C_e represent the initial and equilibrium concentrations of dye in mg/L. V stands for the volume of solution in mL, and W is the mass of the adsorbent in g.

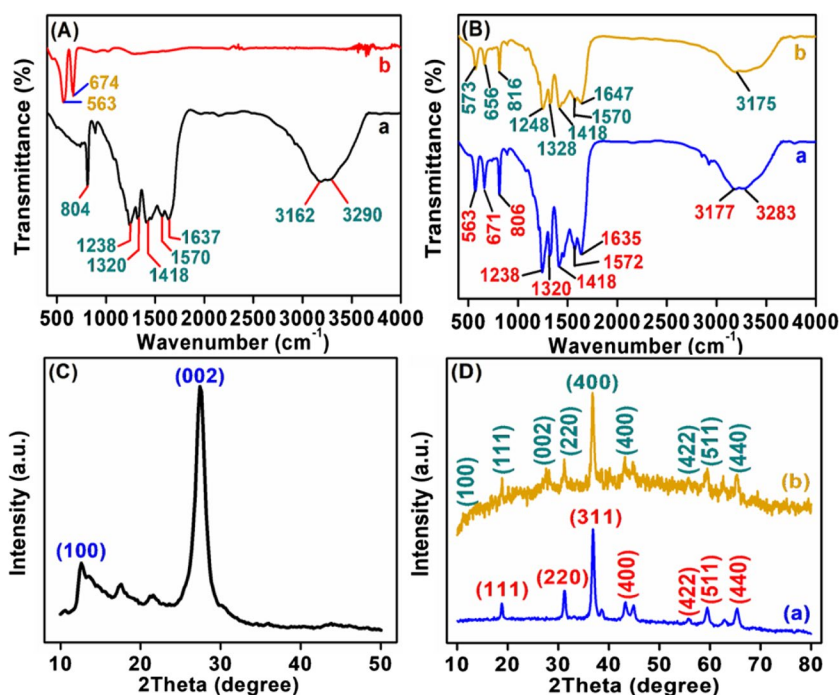
Results and discussion

Material characterizations

FT-IR analysis

The stretching and bending vibrations of different types of bonds and functional groups in the synthesized nanomaterials were studied by employing FT-IR studies. The FT-IR spectrum of $\text{g-C}_3\text{N}_4$ is shown in Fig. 1(A), curve a, where a peak at 1570 cm^{-1} was observed for heptazine units, while the characteristic peaks at 1418 and 804 cm^{-1} were due to the ring modes of the s-triazine unit. The presence of broad bands at 3162 and 3290 cm^{-1} was related to the N–H stretching vibrations. The typical C–N stretching frequencies were observed at 1238 and 1320 cm^{-1} while C=N stretching vibration was recorded at 1637 cm^{-1} owing to the presence of sp^2 bonded carbon atoms (Singh et al. 2022c)(Xu et al. 2017). The characteristic FT-IR spectrum of NiCo_2O_4 is shown in Fig. 1(A), curve b, where, two sharp peaks at 563 and 674 cm^{-1} , were correlated to the ν_1 and ν_2 stretching vibrations of the metal-oxygen bond in nickel-cobalt spinel oxide (Abu-Zied et al. 2014). The FT-IR spectrum of the $\text{NiCo}_2\text{O}_4@ \text{g-C}_3\text{N}_4$ as illustrated in Fig. 1(B), curve a, shows the existence of representative peaks of both $\text{g-C}_3\text{N}_4$ and NiCo_2O_4 with little changes in their respective percentage transmittance and thus confirms the successful preparation of the $\text{NiCo}_2\text{O}_4@ \text{g-C}_3\text{N}_4$ nanocomposite. Further, the FT-IR spectrum of $\text{NiCo}_2\text{O}_4@ \text{g-C}_3\text{N}_4$ nanocomposite after adsorption of FGD is shown in Fig. 1(B), curve b, where the peaks at 563 , 671 , 806 , 1238 , 1320 and 1635 cm^{-1} were shifted to 573 , 656 , 816 , 1248 , 1328 and 1647 cm^{-1} owing to the weak interaction between FGD and $\text{NiCo}_2\text{O}_4@ \text{g-C}_3\text{N}_4$ nanocomposite.

Fig. 1 FT-IR spectra of (A) $g\text{-C}_3\text{N}_4$ (a) and NiCo_2O_4 (b); (B) $\text{NiCo}_2\text{O}_4@g\text{-C}_3\text{N}_4$ nanocomposite (a) and $\text{NiCo}_2\text{O}_4@g\text{-C}_3\text{N}_4$ nanocomposite after adsorption (b). XRD patterns of (C) $g\text{-C}_3\text{N}_4$, and (D) NiCo_2O_4 (a) and $\text{NiCo}_2\text{O}_4@g\text{-C}_3\text{N}_4$ nanocomposite (b)



XRD studies

The crystallinity or amorphous properties of the prepared materials were examined through powder XRD. The XRD spectrum of $g\text{-C}_3\text{N}_4$ is illustrated in Fig. 1(C), where the appearance of a sharp and intense peak at $2\theta = 27.37^\circ$ is due to the reflection from the (002) interplane, while a small peak at $2\theta = 12.60^\circ$ is due to the (100) inplanar reflection from $g\text{-C}_3\text{N}_4$ sheets (JCPDS file No. 87–1526) (Kumar et al. 2016; Singh et al. 2021). The XRD analysis of NiCo_2O_4 as represented in Fig. 1(D), curve a, shows the presence of diffraction peaks at 2θ values of 18.81° , 31.26° , 36.91° , 43.14° , 55.78° , 59.41° , and 65.33° ; those were related to (111), (220), (311), (400), (422), (511), and (440) crystal planes, respectively (Kaur et al. 2022b). The obtained diffraction pattern for NiCo_2O_4 was in accordance with JCPDS card No. 73–1702) (Varalakshmi et al. 2021). The XRD spectrum of the synthesized hybrid material (*c.f.* Figure 1(D), curve b) shows the presence of characteristic diffraction peaks of $g\text{-C}_3\text{N}_4$ and NiCo_2O_4 , confirming the preparation of $\text{NiCo}_2\text{O}_4@g\text{-C}_3\text{N}_4$ nanocomposite.

Morphological characteristics

The surface properties of the synthesized nanomaterials were examined through SEM. The SEM image of $g\text{-C}_3\text{N}_4$ as depicted in Fig. 2(A) shows the presence of layered sheets and some irregular flakes (Singh et al. 2022a). The microstructures of NiCo_2O_4 nanoparticles as depicted in Fig. 2(B) show the presence of grains like agglomerated

nano-crystals (Kaur et al. 2022b). The NiCo_2O_4 nanoparticles are evenly scattered on the sheets of $g\text{-C}_3\text{N}_4$ in the produced $\text{NiCo}_2\text{O}_4@g\text{-C}_3\text{N}_4$ nanocomposite, as represented in Fig. 2(C). Moreover, the EDX spectrum shows sharp peaks for C, N, and O elements in $g\text{-C}_3\text{N}_4$ (Fig. 2D); Ni, Co, and O elements in NiCo_2O_4 (Fig. 2E); and C, N, O, Ni, and Co elements in $\text{NiCo}_2\text{O}_4@g\text{-C}_3\text{N}_4$ nanocomposite (Fig. 2F).

The TEM images of the produced nanomaterials were captured to study the shapes and sizes of the particles or flakes. The sheets of $g\text{-C}_3\text{N}_4$ are irregular or round-shaped flakes and stacked in the form of a graphite-like assembly, as observed from the TEM analysis of $g\text{-C}_3\text{N}_4$ (*c.f.* Figure 3A) (Singh et al. 2022a)(Ahmad et al. 2020). The NiCo_2O_4 nanoparticles are spherical, hexagonal, and some irregular shaped, as shown in the TEM image of NiCo_2O_4 (*c.f.* Figure 3B) with a wide distribution of particle sizes lying in the range of nanoscale (Palani et al. 2022). The uniformly distributed NiCo_2O_4 nanoparticles on the flakes of $g\text{-C}_3\text{N}_4$ as observed in the TEM image of $\text{NiCo}_2\text{O}_4@g\text{-C}_3\text{N}_4$ nanocomposite (*c.f.* Figure 3C) might separate the neighboring sheets and provide a highly effective surface area. Furthermore, the selected area electron diffraction (SAED) patterns of $g\text{-C}_3\text{N}_4$ (Fig. 3D) and NiCo_2O_4 (Fig. 3E) have shown their amorphous and polycrystalline natures, respectively. The SAED pattern of $\text{NiCo}_2\text{O}_4@g\text{-C}_3\text{N}_4$ nanocomposite is shown in Fig. 3(F), where alternating bright and dark rings along with bright spots were recorded.

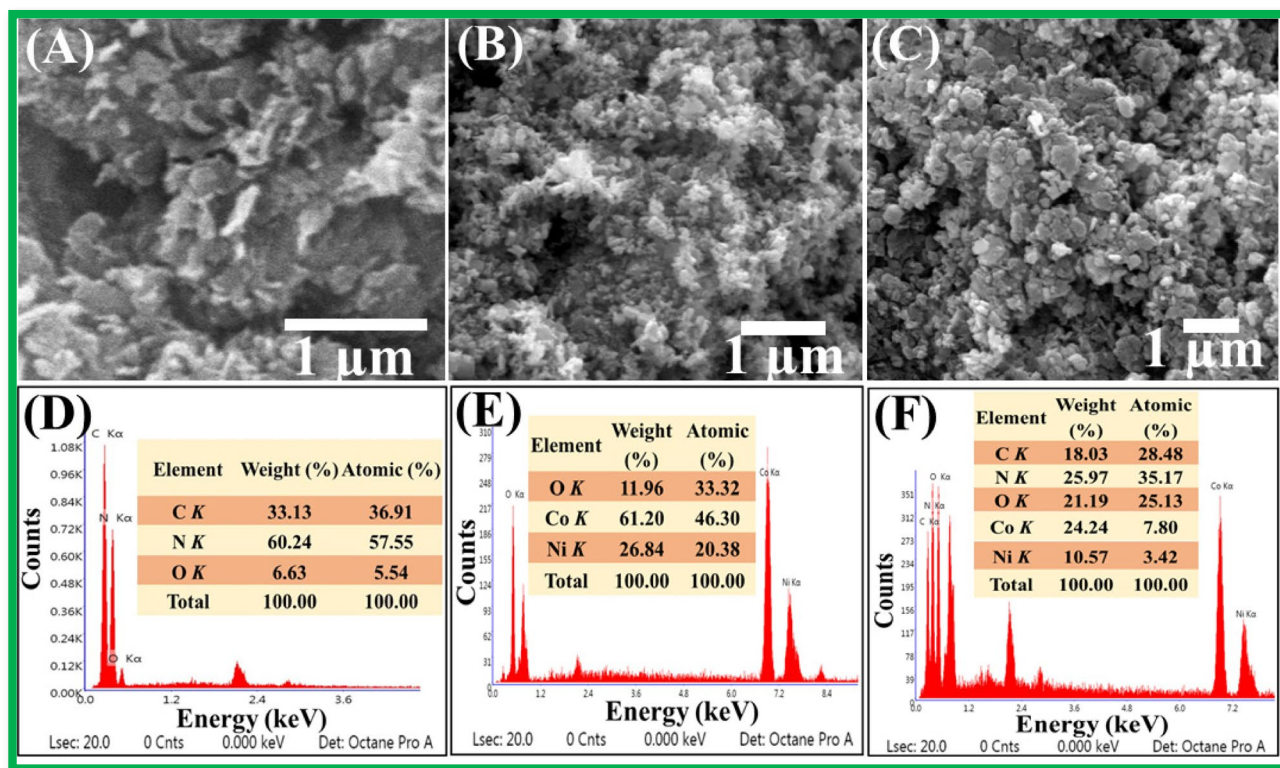


Fig. 2 SEM images of (A) g-C₃N₄, (B) NiCo₂O₄ and (C) NiCo₂O₄@g-C₃N₄ nanocomposite. EDX analysis of (D) g-C₃N₄, (E) NiCo₂O₄ and (F) NiCo₂O₄@g-C₃N₄ nanocomposite

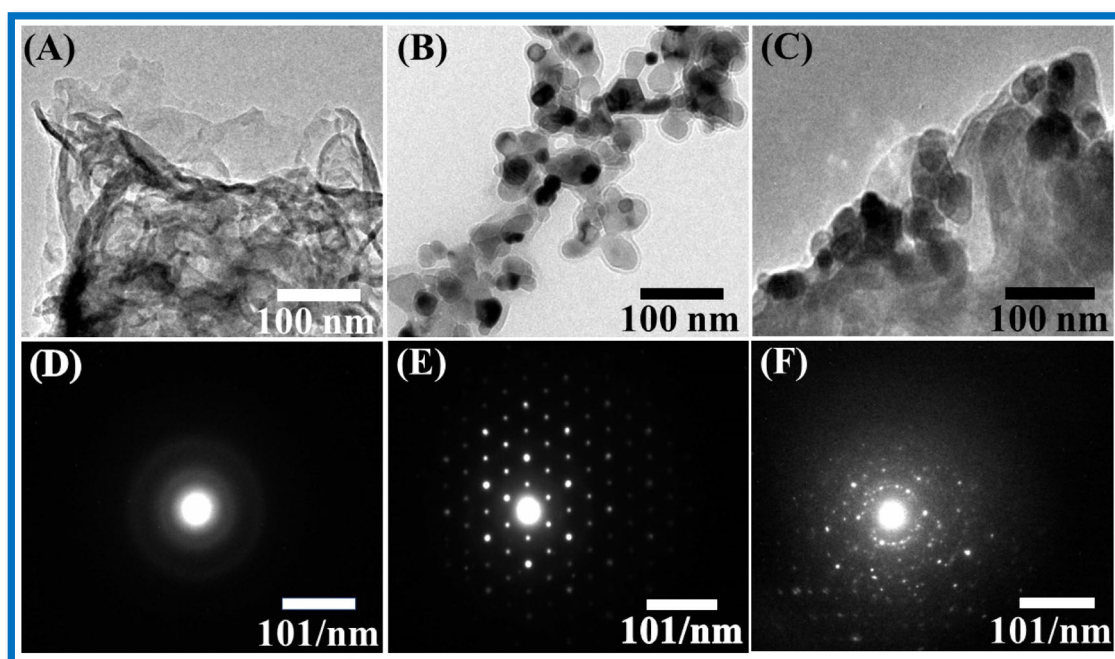


Fig. 3 TEM images of (A) g-C₃N₄, (B) NiCo₂O₄ and (C) NiCo₂O₄@g-C₃N₄ nanocomposite. SAED pattern of (D) g-C₃N₄, (E) NiCo₂O₄ and (F) NiCo₂O₄@g-C₃N₄ nanocomposite

Adsorption results

Effect of pH

The influence of pH on the adsorption of dye was investigated by varying the pH range from 2 to 10 with a known amount of dye solution in the presence of an optimized dose (50 mg) of adsorbent, and the obtained UV–visible spectra at the respective pH are represented in Fig. 4(A). The decolorization of dye solution reduced with a rise in pH, as shown in Fig. 4(B), and a maximum removal of 95.38% was obtained at pH 2. This can be explained on the basis that, at $\text{pH} < \text{pH}_{\text{zpc}}$, the $\text{NiCo}_2\text{O}_4@\text{g-C}_3\text{N}_4$ nanocomposite acquires a positive charge due to protonation, which favors the adsorption of negatively charged FGD. However, the rate of adsorption decreased with an increase in pH owing to the loss of electrostatic interaction between the adsorbent and FGD. The presence of a negative charge on the surface of a nanocomposite at $\text{pH} > \text{pH}_{\text{zpc}}$ due to the accumulation of hydroxide ions from the water molecule disfavored the adsorption phenomenon (Nizam et al. 2021). Thus, the pH of the solution was maintained at 2 for further studies.

Effect of contact time

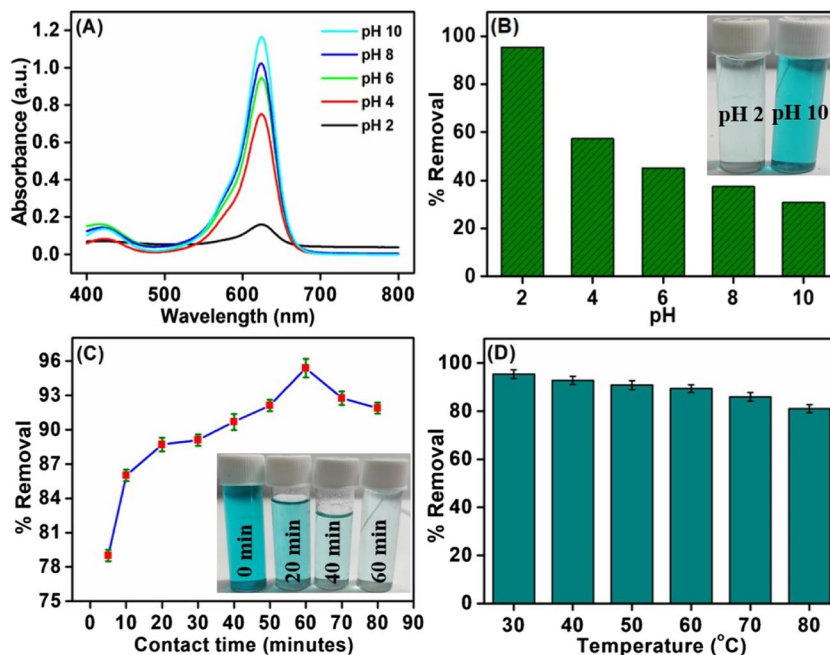
The contact time was optimised for efficient removal of dye by examining the impact of the time range of 5 to 80 min on the adsorption of FGD in the presence of an optimized dose (50 mg) of $\text{NiCo}_2\text{O}_4@\text{g-C}_3\text{N}_4$ at pH 2.0. The obtained results are denoted in Fig. 4(C), where it was obtained that there was a rapid increase in adsorption with enhanced contact

time, and then the removal of dye increased gradually till equilibrium was achieved. There was very quick removal of dye at the initial stage, and about 80% of the dye solution was decolorized within 5 min of interaction between the adsorbent and dye solution owing to the presence of a larger number of active sites in the starting phase of adsorption. The maximum removal of FGD was found to be 95.38% at 60 min and then decolourisation of dye solution was slightly decreased owing to the desorption of adsorbed dye molecules from the adsorbent with a more increase in contact time (Saad et al. 2012). Thus, further studies were done at an optimised time of 60 min for maximum removal of FGD.

Effect of temperature and thermodynamics of the adsorption

The effect of temperature on the removal of FGD was also studied by varying temperature in the range of 303 to 353 K, and the obtained results are illustrated in Fig. 4(D). It was observed that adsorption was favored at low temperatures and percentage removal decreased with temperature. The maximum removal of 95.38% for FGD was obtained at 303 K (30 °C). The decrease in adsorption with a rise in temperature might be attributed to the disturbance in electrostatic interaction and intermolecular hydrogen bonding, which are responsible for the adsorption of dye on the surface of the adsorbent (Singh et al. 2022b). Further, the solubility of FGD in solution increased with temperature due to the stronger interaction between the dye molecule and the solution compared to the interaction between dye and adsorbent. These obtained results suggest that the adsorption

Fig. 4 (A) UV–visible spectra of FGD after adsorption on $\text{NiCo}_2\text{O}_4@\text{g-C}_3\text{N}_4$ nanocomposite at different pH. Effect of (B) pH, inset = image of FGD removal, (C) contact time, inset = image of FGD removal, and (D) temperature on percentage removal of FGD



phenomenon might be an exothermic process. The thermodynamic parameters for the adsorption process were calculated using Van't Hoff Eq. (3) (Singh et al. 2022b).

$$\ln K_d = \frac{\Delta S^\circ}{R} - \frac{\Delta H^\circ}{RT} \quad (3)$$

Here, ΔS° and ΔH° denote the change in entropy and enthalpy, respectively. K_d represents the distribution coefficient, which was calculated by Eq. (4).

$$K_d = \frac{q_e}{C_e} \quad (4)$$

Moreover, the value of the change in free energy (ΔG°) was calculated using Eq. (5).

$$\ln K_d = \frac{-\Delta G^\circ}{RT} \quad (5)$$

The values of ΔH° and ΔS° were calculated from the respective slope and intercept of the $\ln K_d$ vs $1/T$ plot represented in Fig. 5(A). The corresponding values of ΔH° and ΔS° were obtained to be $-26.25 \text{ kJ.mol}^{-1}$ and $-67.64 \text{ J.mol}^{-1} \text{ K}^{-1}$. The negative value of ΔH° confirmed the existence of an exothermic adsorption phenomenon. The obtained thermodynamic parameters are represented in Table S1.

Adsorption kinetics

The kinetics for adsorption of FGD at $\text{NiCo}_2\text{O}_4@\text{g-C}_3\text{N}_4$ nanocomposite were studied by fitting the obtained

experimental data to a number of kinetic models like pseudo-first order (c.f. Figure 5B), pseudo-second order (c.f. Figure 5C), and simple first order models (c.f. Figure 5D). The values obtained for various reaction orders are presented in Table S2. The R^2 value for pseudo-second order (0.99) was close to unity, while for pseudo-first order (0.96) and simple first order (0.91), it has shown deviation from unity. Hence, it was inferred that adsorption of FGD at $\text{NiCo}_2\text{O}_4@\text{g-C}_3\text{N}_4$ was governed by pseudo-second order (Singh et al. 2022b)(Ren et al. 2018). Further, there was a wide mismatch between experimental and calculated values of q_e in the case of the pseudo-first order model, and thus, it was not applicable for defining the adsorption process. However, the closely related experimental and calculated q_e values for pseudo-second order have shown their capability to describe the kinetics of FGD adsorption on $\text{NiCo}_2\text{O}_4@\text{g-C}_3\text{N}_4$ nanocomposite.

Adsorption isotherms

The adsorption capacity of the synthesized $\text{NiCo}_2\text{O}_4@\text{g-C}_3\text{N}_4$ nanocomposite towards removal FGD was investigated by fitting the obtained data to four different isotherm models such as Langmuir, Freundlich, Temkin, and Henry models (Verma et al. 2022)(Ren et al. 2018)(Sadegh et al. 2017). The linear C_e/q_e vs C_e plot for the Langmuir model is represented in Fig. 6(A), and the obtained values of slope and intercept were used in the calculation of the maximum monolayer adsorption capacity (q_m) and Langmuir constant (K_L), respectively. The q_m and K_L values were

Fig. 5 (A) $\ln K_d$ vs $1/T$ plot for thermodynamics study and Kinetics plot for (B) pseudo-first order, (C) pseudo-second order and (D) simple first order

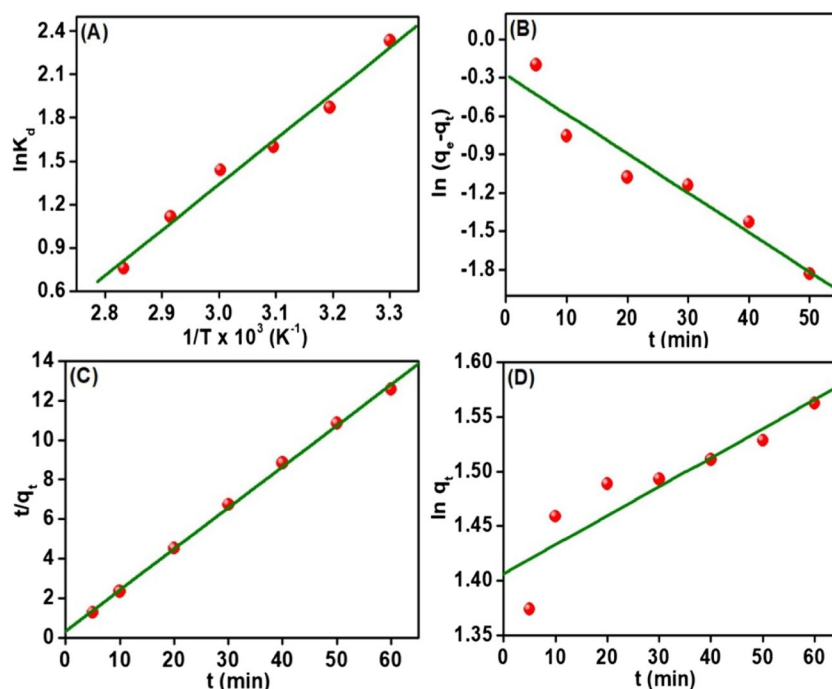
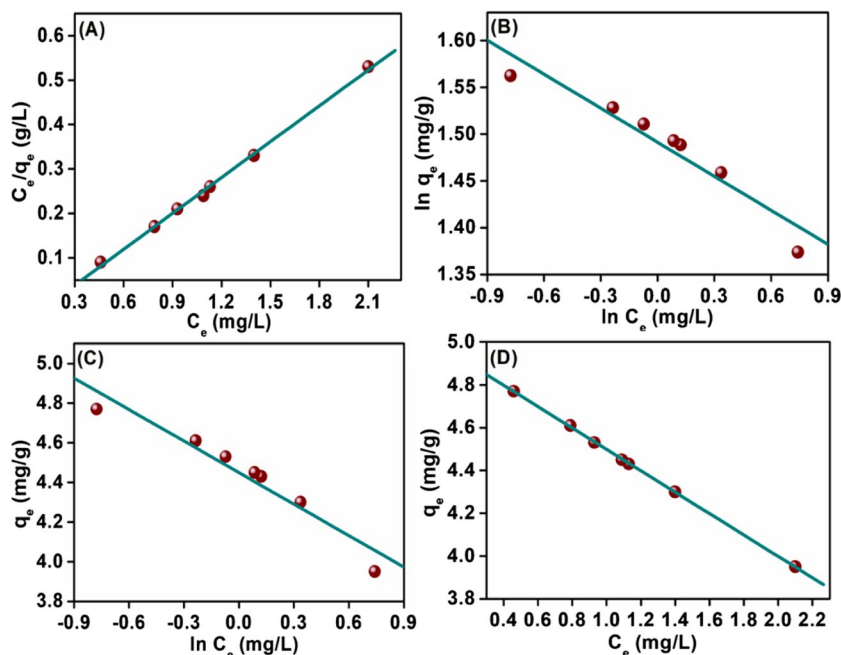


Fig. 6 Adsorption isotherm plots for (A) Langmuir, (B) Freundlich, (C) Temkin, and (D) Henry model



estimated to be 3.71 mg.g^{-1} and 6.35 L.mg^{-1} , respectively. The obtained value of K_L was used to assess the dimensionless equilibrium parameter (R_L) for 10 mg/L of FGD solution, and it was found to be 0.015 , which confirmed the favorable adsorption. Similarly, experimental data were fitted to the Freundlich adsorption isotherm model, and the corresponding $\ln q_e$ vs $\ln C_e$ plot is denoted in Fig. 6(B). The slope and intercept of the plot were used to evaluate the values of n and the Freundlich constant (K_F), respectively. The Temkin and Henry adsorption isotherms were also applied, and the corresponding q_e vs $\ln C_e$ and q_e vs C_e plots are represented in Fig. 6(C) and Fig. 6(D), respectively. The obtained data from fitting to various models is represented in Table S3. The R^2 value of 0.99 was obtained for both Langmuir and Henry models, which has shown better fitting of experimental data compared to the low R^2 value of 0.96 for both Freundlich and Temkin models. Thus, the Langmuir and Henry isotherm models were applicable for the removal of FGD on $\text{NiCo}_2\text{O}_4@g\text{-C}_3\text{N}_4$ nanocomposite, suggesting the monolayer adsorption of dye (Verma et al. 2022). Further, the comparison of maximum adsorption of FGD onto the developed $\text{NiCo}_2\text{O}_4@g\text{-C}_3\text{N}_4$ nanocomposite with various reported works is represented in Table S4.

Mechanism of adsorption

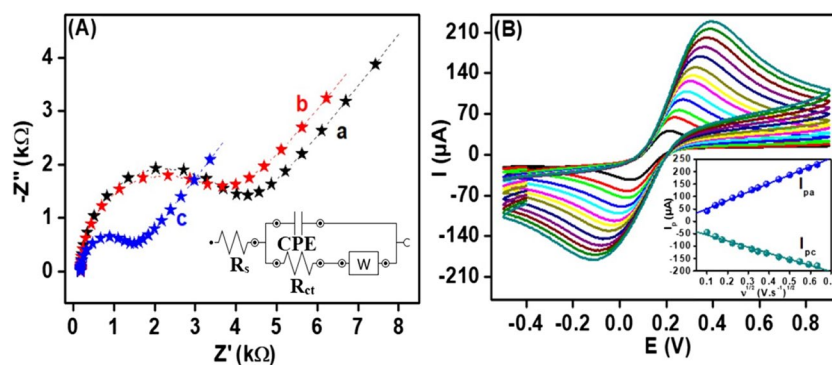
Nanomaterials based adsorbents play an important role in adsorptive removal of dyes from wastewater owing to their large surface to volume ratio. The occurrence of van der Waal forces and electrostatic attractions between the FGD molecules and $\text{NiCo}_2\text{O}_4@g\text{-C}_3\text{N}_4$ nanocomposite are

responsible for elimination of dye molecules from the aqueous solution. The increase in adsorbent dose and contact time upto optimal conditions enhances the decolorization process due to availability of greater number of active sites for adsorbent-adsorbate interactions. Further, anionic nature of FGD prefers the adsorption at pH below pH_{zpc} of the nanocomposite. Thus, all the favorable conditions for the possible interactions enhances the mass transfer of dye molecules on the surface and into the pores of $\text{NiCo}_2\text{O}_4@g\text{-C}_3\text{N}_4$ nanocomposite-based adsorbent.

Electrochemical properties of the fabricated electrodes

The EIS method was utilized to examine the interfacial properties of different modified and unmodified SPCEs. For this, an EIS study was performed in the presence of $5 \text{ mM K}_3[\text{Fe}(\text{CN})_6]/\text{K}_4[\text{Fe}(\text{CN})_6]$ prepared in 0.1 N KCl . The equivalent Randles and Erschler model required for fitting the EIS data to get the corresponding Nyquist plot is represented in the inset to Fig. 7(A). The solution resistance and charge transfer resistance are represented by R_s and R_{ct} , respectively, while the constant phase element (CPE) denotes the double layer capacitance in the equivalent circuit model. W signifies the Warburg impedance, which is produced because of mass diffusion (Singh et al. 2023). The semi-circular region of the EIS plot is observed at a higher frequency which corresponds to the electron transfer phenomenon, whereas the linear part is obtained at a lower frequency owing to the diffusion-controlled process. The values of R_{ct} govern the kinetics of electron transfer, and

Fig. 7 (A) Nyquist plot for bare SPCE (a), g-C₃N₄/SPCE (b), and NiCo₂O₄@g-C₃N₄/SPCE (c), **inset**, equivalent circuit and (B) CV of NiCo₂O₄@g-C₃N₄/SPCE in [Fe(CN)₆]^{3-/4-} at various scan rates, the **inset** I_p vs. $\nu^{1/2}$ plot



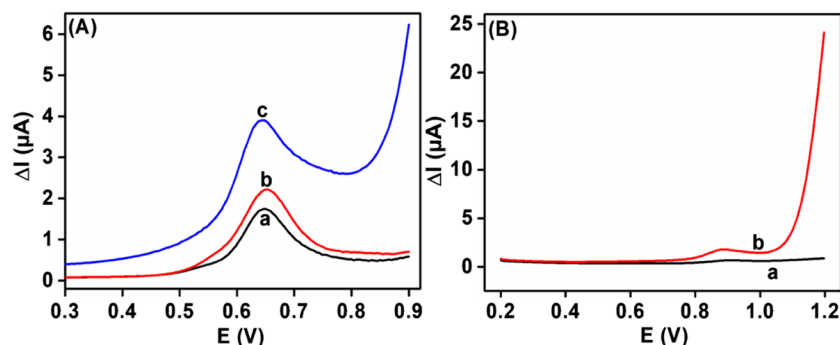
they were interpreted from the semi-circular diameter of the Nyquist plot (Singh et al. 2023)(Agrahari et al. 2022a). The obtained Nyquist plots for various modified and bare electrodes are represented in Fig. 7(A), where the R_{ct} values for bare SPCE (curve a), g-C₃N₄/SPCE (curve b) and NiCo₂O₄@g-C₃N₄/SPCE (curve c) were obtained to be 3.52 kΩ, 3.11 kΩ and 1.15 kΩ, respectively. The value of R_{ct} is lowest for NiCo₂O₄@g-C₃N₄/SPCE. This might be because of facilitated electron transfer owing to the integration of NiCo₂O₄ nanoparticles on the sheets of g-C₃N₄ in the synthesized nanocomposite.

Further, the electroactive surface area of the nanocomposite modified electrode was calculated by carrying out CV studies in 0.1 N KCl containing 5 mM [Fe(CN)₆]^{3-/4-}. The obtained voltammograms at different scan rates in the range of 0.01 to 0.4 V.s⁻¹ are represented in Fig. 7(B). There was linear variation in anodic and cathodic peak current with the square root of scan rate ($\nu^{1/2}$), as represented in the inset to Fig. 7(B) and the obtained corresponding regression equation for current is written as in Eqs. 6 and 7, respectively.

$$I_{pa}(\mu A) = 341.03\nu^{1/2}/(Vs^{-1})^{1/2} + 16.27 \quad (R^2 = 0.9987) \quad (6)$$

$$I_{pc}(\mu A) = -246.31\nu^{1/2}/(Vs^{-1})^{1/2} - 29.89 \quad (R^2 = 0.9937) \quad (7)$$

Fig. 8 (A) DPV response of 50 μM FGD at bare SPCE (a), g-C₃N₄/SPCE (b), and NiCo₂O₄@g-C₃N₄/SPCE (c) in 0.1 M PBS (pH 7.0). (B) DPV response of bare GCE (curve a) and NiCo₂O₄@g-C₃N₄/GCE (curve b) in the presence of 50 μM FGD



The electroactive surface area of NiCo₂O₄@g-C₃N₄/SPCE was calculated using the Randles–Sevcik equation (Eq. 8) (Singh et al. 2021).

$$I_p = 2.69 \times 10^5 n^3/2 AD^{1/2} \nu^{1/2} C \quad (8)$$

Here, I_p , n , A , D , ν , and C represent the peak current, number of transferred electrons (here, $n=1$), active surface area of the electrode, diffusion coefficient (7.6×10^{-6} cm².s⁻¹) of 5.0 mM [Fe(CN)₆]^{3-/4-} in the presence of 0.1N KCl, scan rates, and concentration of solution, respectively. For NiCo₂O₄@g-C₃N₄/SPCE, the electroactive surface area was calculated as 0.174 cm², and it was found to be greater than the geometric surface area of bare SPCE (0.1256 cm²). The increased surface area was attributed to the effective modification of the electrode surface with the synthesized material.

Electrochemical oxidation of FGD

Electrochemical analysis of FGD at various electrodes

The electrochemical response of FGD was analysed at different modified and unmodified SPCEs through DPV in the potential window of 0.2 to 0.9 V. DPV was recorded in the presence of 50 μM FGD in 0.1 M PBS (pH 7.0). The obtained voltammograms are represented in Fig. 8(A). It was observed that oxidation of FGD occurred at 0.65 V on

the surface of bare SPCE (curve a) with a very weak current response. The oxidation of FGD at g-C₃N₄/SPCE (curve b) is observed with a slightly improved current response, which is due to the ease of accessibility of FGD to the surface of g-C₃N₄/SPCE. The oxidation signal for FGD is highest at NiCo₂O₄@g-C₃N₄/SPCE (curve c). The occurrence of highly improved current response at nanocomposite modified SPCE was attributed to the synergistic effect of NiCo₂O₄ and g-C₃N₄ owing to the successful assembly of highly conducting NiCo₂O₄ nanoparticles in the bulk and surface of g-C₃N₄ flakes. Further, the high effective surface area of NiCo₂O₄@g-C₃N₄/SPCE also facilitates diffusion of FGD at the electrode surface. The electrochemical oxidation of FGD was also examined at bare GCE and NiCo₂O₄@g-C₃N₄/GCE through DPV by applying potential in the range of 0.2 to 1.2 V, and the obtained results are shown in Fig. 8(B). A very weak oxidation peak of 50 μM FGD was obtained at 0.88 V on bare GCE (curve a) and nanocomposite modified GCE (curve b). NiCo₂O₄@g-C₃N₄/SPCE has shown lower oxidation potential for FGD compared to NiCo₂O₄@g-C₃N₄/GCE because of the high electrochemical activity of the nanocomposite modified SPCE.

Scan rate studies

The electro-oxidation nature of FGD on the surface of NiCo₂O₄@g-C₃N₄/SPCE was investigated at different scan rates. CV was employed to determine the electrochemical response of 20 μM FGD at NiCo₂O₄@g-C₃N₄/SPCE by varying the scan rates, and the obtained results are represented in Fig. 9(A). It was observed that the oxidation peak current for

FGD increases with an increase in scan rate. The linear variation between I_{pa} and ν^{1/2} as represented in Fig. 9(B) was due to the occurrence of diffusion-controlled processes (Agrahari et al. 2022b). The corresponding linear regression expression for current is written in Eq. 9.

$$I_{pa}(\mu A) = 208.306\nu^{1/2}(\text{V}\cdot\text{s}^{-1})^{1/2} + 3.0135 \quad (R^2 = 0.9985) \quad (9)$$

The value of the slope from the log I_{pa} vs log ν plot (c.f. Figure 9C) was calculated to be 0.56, which confirmed the existence of a diffusion-controlled phenomenon for the oxidation of FGD at the electrode surface. Further, there was linear variation between E_{pa} and log ν as can be observed from the Tafel plot depicted in Fig. 9(D). The linear regression expression for E_{pa} is written as in Eq. 10.

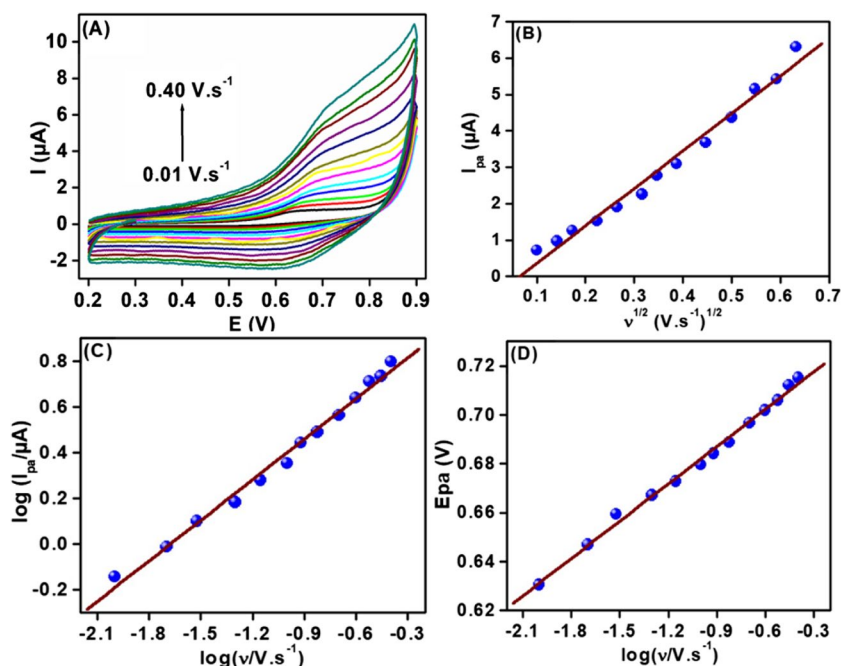
$$E_{pa}(\text{V}) = 0.0946\log\nu(\text{V}\cdot\text{s}^{-1}) + 0.8189 \quad (R^2 = 0.9948) \quad (10)$$

The linear shifts in E_{pa} with an increase in scan rate and the appearance of a broader peak at higher scan rates were caused by irreversible electro-oxidation of FGD at the electrode–electrolyte interface. Moreover, the E_{pa} vs log ν plot along with Eqs. 11 and 12 were used to calculate the value of the electron transfer coefficient (α) (Singh et al. 2021).

$$E_{pa} = \frac{b\log\nu}{2} + \text{constant} \quad (11)$$

$$b = \frac{2.303RT}{(1 - \alpha)nF} \quad (12)$$

Fig. 9 (A) CV of 20 μM FGD at different scan rates. (B) I_{pa} vs. ν^{1/2} plot, (C) log I_{pa} vs. log ν plot, (D) E_{pa} vs. log ν plot



Here, b is the Tafel slope. The value of α for electrochemical oxidation of FGD at the nanocomposite modified SPCE was found to be 0.68 ($n = 1$). This confirmed the presence of a completely irreversible phenomenon for the oxidation of FGD.

The findings from scan rate analysis are in close agreement with the literature reports, and it suggests that the occurrence of a well-resolved anodic response is due to the oxidation of FGD to the quinone form in the selected potential range (Shah 2020)(Shetti and Nayak 2016). The probable pathway for the oxidation of FGD is shown in Fig. S4. During the whole oxidation process, one electron and one proton were irreversibly lost, leaving behind the stable product. The working electrode surface of $\text{NiCo}_2\text{O}_4@g\text{-C}_3\text{N}_4/\text{SPCE}$ might facilitate the transfer of electrons between the FGD molecule and the modified electrode by reducing the activation energy barrier for electro-oxidation of FGD owing to the high electro-active surface area of the nanocomposite modified SPCE.

Determination of FGD

The electroanalytical application of the designed sensor was evaluated to determine various concentrations of FGD in 0.1 M PBS (pH 7.0) at a $g\text{-C}_3\text{N}_4/\text{GN}/\text{SPCE}$ using DPV. The voltammograms obtained for sensing of FGD are illustrated in Fig. 10(A), where a gradual rise in peak current is observed with increasing concentration of FGD. The corresponding calibration plot is represented in Fig. 10(B), where a linear increase in peak current with added concentration of FGD is observed in dual concentration ranges, 0.2 to 10 μM (inset 1) and 10 to 800 μM (inset 2). The linear regression equations for oxidation current in the 0.2 to 10 μM and 10 to 800 μM concentration ranges are written in Eqs. 13 and 14, respectively.

$$\Delta I_{pa}/\mu\text{A} = 0.0868(C/\mu\text{M}) + 0.8360 \quad (R^2 = 0.9969) \quad (13)$$

$$\Delta I_{pa}/\mu\text{A} = 0.0113(C/\mu\text{M}) + 2.3318 \quad (R^2 = 0.9895) \quad (14)$$

Here, C signifies the FGD concentration in μM . The occurrence of a dual concentration range was attributed to the restricted diffusion of the analyte at the surface of

$\text{NiCo}_2\text{O}_4@g\text{-C}_3\text{N}_4/\text{SPCE}$ with the addition of FGD. Moreover, the loss in linearity was noted above the 800 μM concentration of FGD owing to the saturation of the active surface of the developed sensor. A method based on the standard deviation of the blank sample was applied in the determination of the limit of detection (LOD) and limit of quantification (LOQ) at the proposed sensing platform using Eqs. 15 and 16, respectively.

$$LOD = \frac{3s}{b} \quad (15)$$

and,

$$LOQ = \frac{10s}{b} \quad (16)$$

Here, s and b represent the standard deviation of the blank sample and the slope of the calibration plot, respectively. The values of LOD and LOQ were evaluated to be 0.13 μM and 0.44 μM , respectively. The sensitivities for determination of FGD in 0.2 to 10 μM and 10 to 800 μM concentration ranges were obtained to be 0.6912 $\mu\text{A} \cdot \mu\text{M}^{-1} \cdot \text{cm}^{-2}$ and 0.0897 $\mu\text{A} \cdot \mu\text{M}^{-1} \cdot \text{cm}^{-2}$, respectively.

Therefore, the fabricated $\text{NiCo}_2\text{O}_4@g\text{-C}_3\text{N}_4/\text{SPCE}$ can be effectively applied for the electrochemical determination of FGD by employing DPV as a measuring technique. This FGD sensor has exhibited a number of benefits compared to traditional methods in terms of short analysis time, low fabrication cost, simplicity, and reliability for technological applications. The proposed FGD sensor is based on SPCE, and thus, it shows features of portability and in-situ monitoring of FGD. Further, the electrochemical performance of the developed FGD sensor is also compared to the previously published works (Shah 2020) (Shetti and Nayak 2016)(Shokrollahi and Roozestan 2013) (Vachirapatama et al. 2008), as reported in Table 1. The electrochemical oxidation of FGD was reported at a very high potential at bare GCE (0.90 V) (Shetti and Nayak 2016) and at Calix8/Au NPs/GCE (0.84 V) (Shah 2020), however, a much-reduced oxidation potential was observed

Fig. 10 (A) DPV measurement of FGD at $\text{NiCo}_2\text{O}_4@g\text{-C}_3\text{N}_4/\text{SPCE}$. (B) Calibration plot

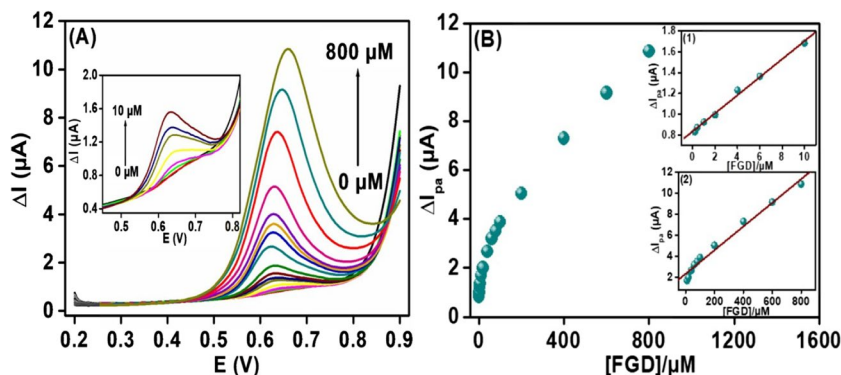


Table 1 Comparison of the developed screen-printed electrochemical sensor with the other existing FGD sensors

Techniques	Electrode	Overpotential (V)	LOD (μM)	Linear range (μM)	References
HPLC	-	-	1.23	-	(Vachirapatama et al. 2008)
CPE	-	-	22	-	(Shokrollahi and Roozestan 2013)
Scanometry					
CPE	-	-	7	-	(Shokrollahi and Roozestan 2013)
UV–Visible					
DPV	Bare GCE	0.90	0.8	30–200	(Shetti and Nayak 2016)
DPV	Calix8/Au NPs/GCE	0.84	0.019	0.05–45	(Shah 2020)
DPV	NiCo ₂ O ₄ @g-C ₃ N ₄ /SPCE	0.64	0.13	0.2 – 800	This work

at NiCo₂O₄@g-C₃N₄/SPCE (0.64 V) due to the combined effect of NiCo₂O₄, g-C₃N₄, and SPCE. The very low LOD of 0.13 μM for FGD was obtained at NiCo₂O₄@g-C₃N₄/SPCE compared to the LOD found in HPLC (Vachirapatama et al. 2008), CPE Scanometry (Shokrollahi and Roozestan 2013), CPE UV–Visible (Shokrollahi and Roozestan 2013), and at bare GCE (Shetti and Nayak 2016) for FGD sensing, while it was comparable to the LOD found at Calix8/Au NPs/GCE (Shah 2020). However, the present FGD sensor has a wide linear calibration range of 0.2 to 800 μM compared to a very small linear concentration range for all other detection methods reported in the table (Shah 2020)(Shetti and Nayak 2016)(Shokrollahi and Roozestan 2013)(Vachirapatama et al. 2008). Moreover, the NiCo₂O₄@g-C₃N₄/SPCE based FGD sensor is the first electrochemical sensor based on an SCPE for sensitive determination of FGD in a wide calibration range. Thus, the prepared electrochemical sensing platform is comparable to or better than the other reported sensors for the sensitive determination of FGD.

Sensor performance

The electrochemical performance of the developed sensor was assessed by measuring the repeatability, reproducibility, and stability of the NiCo₂O₄@g-C₃N₄/SPCE towards electrochemical oxidation of FGD. The repeatability of the fabricated electrodes was evaluated in the presence of 20 μM FGD using the DPV technique for five successive measurements, and the obtained results are shown in Fig. S6(A). The oxidation response of each cycle was compared with the first measurement, and the corresponding relative standard deviation (RSD) was observed to be 4.92%. The reproducibility of the prepared sensor was examined by measuring the response of 20 μM FGD through DPV on five different electrodes prepared under similar laboratory conditions. The obtained bar diagram is shown in Fig. S6(B) and the RSD

value was found to be 3.80% suggesting only a slight variation in the electrochemical performances of each sensor.

Further, for examining the stability of the fabricated sensor, different NiCo₂O₄@g-C₃N₄/SPCE were prepared at once, and then an oxidation current of 20 μM FGD was measured through DPV for two weeks. The corresponding results are represented in Fig. S6(C), and it was observed that the current response for oxidation FGD decreased by 5.21% and 7.54% with respect to its initial response after one and two weeks, respectively. The decrease in oxidation response was due to the formation of an oxide layer on the working surface of the electrode, and hence, it is recommended to store the prepared electrode in an inert atmosphere. These results have shown exceptional repeatability, reproducibility, and longer storage stability of the prepared sensing platform towards the determination of FGD.

Interference study

The selectivity of NiCo₂O₄@g-C₃N₄/SPCE towards sensitive determination of FGD was examined to check the practical applications of the developed sensor. The interference study was performed by taking 1 μM FGD as a fixed concentration and then adding 100 folds of some common interfering species such as K⁺, Na⁺, Cl⁻, SO₄²⁻, uric acid, hexachlorobenzene, hydroquinone, Rhodamine B, methylene blue, and tartrazine. The response of FGD was measured in the absence and presence of added interferents using DPV in the potential range of 0.2 to 0.9 V. The obtained results are illustrated in the form of a bar diagram in Fig. S6(D), and it was observed that there was no significant influence of added interfering species on the oxidation response of FGD. However, the slight variation in peak potential and current response of FGD was due to the different adsorption or diffusion capacities of the added interfering species. These results have shown the excellent specificity of the sensor towards the determination of FGD in practical samples.

Determination of FGD in real samples

The developed $\text{NiCo}_2\text{O}_4@\text{g-C}_3\text{N}_4/\text{SPCE}$ was tested for its sensing ability in a real sample prepared from collected waste water by diluting it in 0.1 M PBS (pH 7.0) for the detection of FGD. The diluted sample was taken in an electrochemical cell, and the standard addition method was used for recovery analysis by measuring the current response for oxidation of FGD. The different concentrations of FGD, including 2.0, 5.0, 20.0, 100.0, and 200.0 μM , were spiked in the real samples, and then the corresponding responses were recorded by employing DPV in the potential range of 0.2 to 0.9 V. The obtained results are shown in Table 2, where an exceptional percentage recovery of 98 to 106% was observed for FGD in the chosen real sample. Furthermore, the RSD of all the recovery analysis was obtained in the range of 0.78 to 2.35%. The excellent percentage recovery with acceptable RSD suggests the absence of any considerable matrix effect, and thus, it shows the potential of the sensor for the detection of FGD in waste water samples with unparalleled sensitivity.

Conclusions

To sum up, this study reported the successful synthesis of $\text{NiCo}_2\text{O}_4@\text{g-C}_3\text{N}_4$ nanocomposite as a low-cost and highly efficient bi-functional material through ultrasonic-assisted reflux methodology for electrochemical monitoring and adsorptive removal of FGD. The prepared nanocomposite has shown effective adsorption behavior towards 95.38% removal of FGD at optimal conditions. The decolorization of FGD solution was favored at a low temperature (303 K) at optimized dose (50 mg), pH (2.0), and time (60 min). The value of ΔG° was found to be negative, suggesting the spontaneous nature of the adsorption phenomenon. The adsorption of dye at $\text{NiCo}_2\text{O}_4@\text{g-C}_3\text{N}_4$ nanocomposite was best fitted with a pseudo-second order model ($R^2=0.99$) and was following the Langmuir adsorption isotherm ($R^2=0.99$). Furthermore, $\text{NiCo}_2\text{O}_4@\text{g-C}_3\text{N}_4$ nanocomposite was incorporated on the SPCE as an electrode modifying material to develop a sensitive and reliable sensing platform for electrochemical determination of FGD. The proposed sensor has shown excellent

selectivity with a sensitivity of $0.6912 \mu\text{A} \cdot \mu\text{M}^{-1} \cdot \text{cm}^{-2}$ and high reproducibility (RSD = 3.80%). The exceptional electrochemical response of the fabricated sensor might be attributed to the effective surface area (0.174 cm^2) and high electrical conductivity of the $\text{NiCo}_2\text{O}_4@\text{g-C}_3\text{N}_4$ nanocomposite. The prepared FGD sensor was also tested for detection of FGD in wastewater, with an excellent recovery between 98.0 and 106%. The success of this nanocomposite as a dual role of adsorbent and electrode material may open up a new strategy for the development of some other $\text{g-C}_3\text{N}_4$ based nanocomposite that may be used in the adsorption and sensing of any environmentally relevant compounds.

Abbreviations FGD: Fast Green dye; SPCE: Screen printed carbon electrode; NiCo_2O_4 : Nickel cobaltite; $\text{g-C}_3\text{N}_4$: Graphitic carbon nitride; GCE: Glassy carbon electrode; CPE: Constant phase element; K_L : Langmuir constant; K_F : Freundlich constant; DPV: Differential pulse voltammetry; EIS: Electrochemical impedance spectroscopy; Calix8/Au NPs/GCE: Calixarene and gold nanoparticles modified GCE

Supplementary Information The online version contains supplementary material available at <https://doi.org/10.1007/s11356-023-30373-3>.

Acknowledgements A K S (Chem./2018-19/RET/Sept.18-term/1/4809) and S A (Chem./2019-2020/RET-2/Sept.19-term/1/975) are thankful to UGC, New Delhi for providing their research fellowships. The fundings received from IOE, BHU are highly acknowledged. Prof. N. V. C. Rao, Department of Geology, BHU, is acknowledged for SEM and EDX measurements. Department of Physics, BHU, is thanked for TEM analysis. We are thankful to Mr. Swetank Shekhar for help during experimental work.

Author contributions AKS: Conceptualization, Methodology, Writing- original draft, Formal analysis; SA: Writing- Review & Editing, data curation; RKG: Investigation, Visualization; IT: Supervision, Validation.

Funding Not applicable.

Data availability Most data generated or analysed during this study are included in this published article and its supplementary information file.

Declarations

Ethical approval Not applicable.

Consent to participate Not applicable.

Consent for publication Not applicable.

Competing interests “The authors have no relevant financial or non-financial interests to disclose.”

References

- Abdi S, Nasiri M (2018) Removal of Fast Green FCF dye from aqueous solutions using Flower Gel as a low-cost adsorbent. *Water Sci Technol* 77:1213–1221. <https://doi.org/10.2166/wst.2017.633>

Table 2 Analysis of FGD in real sample at $\text{NiCo}_2\text{O}_4@\text{g-C}_3\text{N}_4/\text{SPCE}$

Samples	Spiked (μM)	Found (μM)	Recovery (%)	RSD (%) n=3)
Waste water	2.0	2.12	106.0	0.78
	5.0	4.92	98.4	1.62
	20.0	21.00	105.0	2.35
	100.0	102.0	102.0	0.86
	200.0	196.0	98.0	2.04

- Abu-Zied BM, Soliman SA, Abdellah SE (2014) Pure and Ni-substituted Co₃O₄ spinel catalysts for direct N₂O decomposition. *Cuihua Xuebao/chinese J Catal* 35:1105–1112. [https://doi.org/10.1016/s1872-2067\(14\)60058-9](https://doi.org/10.1016/s1872-2067(14)60058-9)
- Agrahari S, Singh AK, Gautam RK, Tiwari I (2022a) Voltammetric analysis of epinephrine using glassy carbon electrode modified with nanocomposite prepared from Co-Nd bimetallic nanoparticles, alumina nanoparticles and functionalized multiwalled carbon nanotubes. *Environ Sci Pollut Res*. <https://doi.org/10.1007/s11356-022-23660-y>
- Agrahari S, Singh AK, Gautam RK, Tiwari I (2022b) Fabrication of gadolinium decorated spherical zinc oxide attached on carbon nanotubes (Gd@ZnO-MWCNTs) for electrochemical detection of a bisphenol derivative BPSIP in real sample matrices. *J Appl Electrochem* 1:3. <https://doi.org/10.1007/s10800-022-01768-w>
- Ahmad R, Tripathy N, Khosla A, et al (2020) Review — Recent Advances in Nanostructured Graphitic Carbon Nitride as a Sensing Material for Heavy Metal Ions Review — Recent Advances in Nanostructured Graphitic Carbon Nitride as a Sensing Material for Heavy Metal Ions. <https://doi.org/10.1149/2.0192003JES>
- Ahmed R, Hossain MA (2021) Optimization of a fixed bed column adsorption of Fast Green dye on used black tea leaves from aqueous solution. *J Iran Chem Soc*. <https://doi.org/10.1007/s13738-021-02310-z>
- Anu Prathap MU, Srivastava R (2013) Electrochemical reduction of lindane (γ -HCH) at NiCo₂O₄ modified electrode. *Electrochim Acta* 108:145–152. <https://doi.org/10.1016/J.ELECTACTA.2013.06.122>
- Arora AK, Jaswal VS, Singh K, Singh R (2016) Metal/Mixed Metal Oxides and their Applications as Adsorbents. *Int J Chem Sci* 14:3215–3227
- Beitollahi H, Garkani Nejad F, Dourandish Z, Tajik S (2022) A novel voltammetric amaranth sensor based on screen printed electrode modified with polypyrrole nanotubes. *Environ Res* 214:113725. <https://doi.org/10.1016/J.ENVRES.2022.113725>
- Christ-Ribeiro A, Maciel JV, Bier EM et al (2022) Application of Electrochemical Sensors in the Determination of Synthetic Dyes in Foods or Beverages and Their Toxicological Effects on Human Health: a Review. *Food Anal Methods* 15:2394–2413. <https://doi.org/10.1007/s12161-022-02282-7>
- Dahiya S, Sharma A, Chaudhary S (2023a) Synthesis of phytoextract-mediated Ag-doped graphitic carbon nitride (Ag@GCN) for photocatalytic degradation of dyes. *Environ Sci Pollut Res* 30:25650–25662. <https://doi.org/10.1007/s11356-023-25359-0>
- Dahiya S, Sharma R, Gautam P et al (2023) Eco-friendly phytofabrication of Ficus Benjamina L. based ZnO-doped g-C₃N₄ nanocomposites for remarkable photocatalysis and antibacterial applications. *Chemosphere* 339:139707. <https://doi.org/10.1016/J.CHEMOSPHERE.2023.139707>
- Fazio E, Spadaro S, Corsaro C, et al (2021) Metal-oxide based nanomaterials: Synthesis, characterization and their applications in electrical and electrochemical sensors. *Sensors* 21. <https://doi.org/10.3390/s21072494>
- Gautam RK, Jaiswal N, Singh AK, Tiwari I (2021) Ultrasound-enhanced remediation of toxic dyes from wastewater by activated carbon-doped magnetic nanocomposites: analysis of real wastewater samples and surfactant effect. *Environ Sci Pollut Res* 28:36680–36694. <https://doi.org/10.1007/s11356-021-13256-3>
- Kaur M, Chand P, Anand H (2022a) Facile synthesis of NiCo₂O₄ nanostructure with enhanced electrochemical performance for supercapacitor application. *Chem Phys Lett* 786:139181. <https://doi.org/10.1016/j.cplett.2021.139181>
- Kaur M, Chand P, Anand H (2022b) Facile synthesis of NiCo₂O₄ nanostructure with enhanced electrochemical performance for supercapacitor application. *Chem Phys Lett* 786:139181. <https://doi.org/10.1016/j.cplett.2021.139181>
- Khan MN, Sarwar A (2007) Determination of points of zero charge of natural and treated adsorbents. *Surf Rev Lett* 14:461–469. <https://doi.org/10.1142/S0218625X07009517>
- Kumar A, Kumar P, Joshi C, Boukherroub R (2016) Nickel Decorated on Phosphorous-Doped Carbon Nitride as an Efficient Photocatalyst for Reduction of Nitrobenzenes. *Nanomaterials* 6:59. <https://doi.org/10.3390/nano6040059>
- Lashanizadegan M, Esfandiari Z, Mirzazadeh H (2019) Evaluation performance of Fe-Mn-Ce-O mixed metal oxides and Fe-Mn-Ce-O/Montmorillonite for adsorption of azo dyes in aqueous solution and oxidation reaction. *Mater Res Express* 6. <https://doi.org/10.1088/2053-1591/ab5550>
- Muinde VM, Onyari JM, Wamalwa B, Wabomba JN (2020) Adsorption of malachite green dye from aqueous solutions using mesoporous chitosan-zinc oxide composite material. *Environ Chem Ecotoxicol* 2:115–125. <https://doi.org/10.1016/J.ENCECO.2020.07.005>
- Nizam NUM, Hanafiah MM, Mahmoudi E et al (2021) The removal of anionic and cationic dyes from an aqueous solution using biomass-based activated carbon. *Sci Rep* 11:1–17. <https://doi.org/10.1038/s41598-021-88084-z>
- Palani R, Wu Y, Wu S et al (2022) Electrochimica Acta Metal-organic framework-derived ZrO₂ / NiCo₂O₄ / graphene mesoporous cake-like structure as enhanced bifunctional electrocatalytic cathodes for long life Li-O₂ batteries. *Electrochim Acta* 412:140147. <https://doi.org/10.1016/j.electacta.2022.140147>
- Panchal P, Malik R, Paul DR et al (2019a) Photocatalytic Activity of Green Synthesized AgCl Nanoparticles Towards E. coli Bacteria. *J Nanosci Nanotechnol* 19:5249–5255. <https://doi.org/10.1166/jnn.2019.16839>
- Panchal P, Paul DR, Sharma A et al (2019b) Phytoextract mediated ZnO/MgO nanocomposites for photocatalytic and antibacterial activities. *J Photochem Photobiol A Chem* 385:112049. <https://doi.org/10.1016/J.JPHOTOCHEM.2019.112049>
- Panchal P, Paul DR, Sharma A et al (2020) Biogenic mediated Ag/ZnO nanocomposites for photocatalytic and antibacterial activities towards disinfection of water. *J Colloid Interface Sci* 563:370–380. <https://doi.org/10.1016/J.JCIS.2019.12.079>
- Panchal P, Meena P, Nehra SP (2021) A rapid green synthesis of Ag/AgCl-NC photocatalyst for environmental applications. *Environ Sci Pollut Res* 28:3972–3982. <https://doi.org/10.1007/s11356-020-11834-5>
- Panchal P, Paul DR, Gautam S et al (2022) Photocatalytic and antibacterial activities of green synthesized Ag doped MgO nanocomposites towards environmental sustainability. *Chemosphere* 297:134182. <https://doi.org/10.1016/J.CHEMOSPHERE.2022.134182>
- Paul DR, Sharma R, Nehra SP, Sharma A (2019a) Effect of calcination temperature, pH and catalyst loading on photodegradation efficiency of urea derived graphitic carbon nitride towards methylene blue dye solution. *RSC Adv* 9:15381–15391. <https://doi.org/10.1039/c9ra02201e>
- Paul DR, Sharma R, Panchal P et al (2019b) Silver Doped Graphitic Carbon Nitride for the Enhanced Photocatalytic Activity Towards Organic Dyes. *J Nanosci Nanotechnol* 19:5241–5248. <https://doi.org/10.1166/jnn.2019.16838>
- Paul DR, Gautam S, Panchal P et al (2020a) ZnO-Modified g-C₃N₄: A Potential Photocatalyst for Environmental Application. *ACS Omega* 5:3828–3838. <https://doi.org/10.1021/acsomega.9b02688>
- Paul DR, Sharma R, Panchal P et al (2020b) Synthesis, characterization and application of silver doped graphitic carbon nitride as photocatalyst towards visible light photocatalytic hydrogen evolution. *Int J Hydrogen Energy* 45:23937–23946. <https://doi.org/10.1016/j.ijhydene.2019.06.061>
- Paul DR, Sharma R, Sharma A, Nehra SP (2022b) Li doped graphitic carbon nitride based solar light responding photocatalyst for

- organic water pollutants degradation. *Proc Indian Natl Sci Acad* 88:696–704
- Paul DR, Sharma R, Singh S et al (2023) Mg/Li Co-doped g-C₃N₄: An excellent photocatalyst for wastewater remediation and hydrogen production applications towards sustainable development. *Int J Hydrog Energy*. <https://doi.org/10.1016/j.IJHYDENE.2022.12.178>
- Paul DR, Sharma R, Rao VS, et al (2022a) Mg/Li@GCN as highly active visible light responding 2D photocatalyst for wastewater remediation application. *Environ Sci Pollut Res* 3–10. <https://doi.org/10.1007/s11356-022-21203-z>
- Rahman MM, Alam MM, Asiri AM (2019) Potential application of mixed metal oxide nanoparticle-embedded glassy carbon electrode as a selective 1,4-dioxane chemical sensor probe by an electrochemical approach. *RSC Adv* 9:42050–42061. <https://doi.org/10.1039/c9ra09118a>
- Rao VS, Sharma R, Paul DR et al (2023) Architecting the Z-scheme heterojunction of Gd₂O₃/g-C₃N₄ nanocomposites for enhanced visible-light-induced photoactivity towards organic pollutants degradation. *Environ Sci Pollut Res*. <https://doi.org/10.1007/s11356-023-25360-7>
- Ren B, Xu Y, Zhang L, Liu Z (2018) Carbon-doped graphitic carbon nitride as environment-benign adsorbent for methylene blue adsorption: Kinetics, isotherm and thermodynamics study. *J Taiwan Inst Chem Eng* 88:114–120. <https://doi.org/10.1016/j.jtice.2018.03.041>
- Saad DMG, Cukrowska EM, Tutu H (2012) Phosphonated cross-linked polyethylenimine for selective removal of uranium ions from aqueous solutions. *Water Sci Technol* 66:122–129. <https://doi.org/10.2166/wst.2012.133>
- Sadegh H, Ali GAM, Gupta VK et al (2017) The role of nanomaterials as effective adsorbents and their applications in wastewater treatment. *J Nanostructure Chem* 7:1–14. <https://doi.org/10.1007/s40097-017-0219-4>
- Shah A (2020) A Novel Electrochemical Nanosensor for the Simultaneous Sensing of Two Toxic Food Dyes. *ACS Omega* 5:6187–6193. <https://doi.org/10.1021/acsomega.0c00354>
- Sharma R, Almasi M, Nehra SP et al (2022) Photocatalytic hydrogen production using graphitic carbon nitride (GCN): A precise review. *Renew Sustain Energy Rev* 168:112776. <https://doi.org/10.1016/j.rser.2022.112776>
- Shetti NP, Nayak DS (2016) Electro-oxidation of a Food Dye Fast Green FCF and Its Analytical Applications. *Anal Bioanal Electrochem* 8:38–50
- Shokrollahi A, Roozestan T (2013) CPE-Scanometry as a new technique for the determination of dyes: Application for the determination of fast green FCF dye and comparison with spectrophotometric results. *Anal Methods* 5:4824–4831. <https://doi.org/10.1039/c3ay40183a>
- Shoran S, Chaudhary S, Sharma A (2022) Photocatalytic dye degradation and antibacterial activities of CeO₂/g-C₃N₄ nanomaterials for environmental applications. *Environ Sci Pollut Res*. <https://doi.org/10.1007/s11356-022-23815-x>
- Shoran S, Sharma A, Chaudhary S (2023) Visible light enhanced photocatalytic degradation of organic pollutants with SiO₂/g-C₃N₄ nanocomposite for environmental applications. *Environ Sci Pollut Res*. <https://doi.org/10.1007/s11356-022-24837-1>
- Singh AK, Jaiswal N, Gautam RK, Tiwari I (2021) Development of g-C₃N₄/Cu-DTO MOF nanocomposite based electrochemical sensor towards sensitive determination of an endocrine disruptor BPSIP. *J Electroanal Chem* 887:115170. <https://doi.org/10.1016/j.jelechem.2021.115170>
- Singh AK, Agrahari S, Gautam RK, Tiwari I (2022a) Fabrication of an innovative electrochemical sensor based on graphene-coated silver nanoparticles decorated over graphitic carbon nitride for efficient determination of estradiol. *Environ Sci Pollut Res*. <https://doi.org/10.1007/s11356-022-23410-0>
- Singh AK, Gautam RK, Agrahari S et al (2022b) Graphene oxide supported Fe₃O₄-MnO₂ nanocomposites for adsorption and photocatalytic degradation of dyestuff: ultrasound effect, surfactants role and real sample analysis. *Int J Environ Anal Chem* 00:1–27. <https://doi.org/10.1080/03067319.2022.2091930>
- Singh AK, Gautam RK, Agrahari S, Tiwari I (2022c) Oxidized g-C₃N₄ decorated with Cu–Al layered double hydroxide as a sustainable electrochemical sensing material for quantification of diclofenac. *Mater Chem Phys* 294:127002. <https://doi.org/10.1016/j.matchemphys.2022.127002>
- Singh AK, Jaiswal N, Tiwari I, et al (2023) Electrochemical biosensors based on in situ grown carbon nanotubes on gold microelectrode array fabricated on glass substrate for glucose determination. *Microchim Acta* 190. <https://doi.org/10.1007/s00604-022-05626-6>
- Sudha V, Senthil Kumar SM, Thangamuthu R (2020) NiCo₂O₄ nanorod: Synthesis and electrochemical sensing of carcinogenic hydrazine. *Inorg Chem Commun* 116:107927. <https://doi.org/10.1016/j.inoche.2020.107927>
- Tahir H, Hamed U, Jahanzeb Q, Sultan M (2008) Removal of fast green dye (C.I. 42053) from an aqueous solution using *Azadirachta indica* leaf powder as a low-cost adsorbent. *Afr J Biotechnol* 7:3906–3911
- Vachirapatana N, Mahajaroensiri J, Visessanguan W (2008) Identification and determination of seven synthetic dyes in foodstuffs and soft drinks on monolithic C18 column by high performance liquid chromatography. *J Food Drug Anal* 16:77–82. <https://doi.org/10.38212/2224-6614.2323>
- Varalakshmi N, Narayana AL, Hussain OM, Sreedhar NY (2021) Improved supercapacitive performance of low pore size and highly stable nanostructured NiCo₂O₄ electrodes. *J Solid State Electrochem* 25:1411–1420. <https://doi.org/10.1007/s10008-021-04911-3>
- Verma S, Pandey CM, Kumar D (2022) A highly efficient rGO grafted MoS₂ nanocomposite for dye adsorption and electrochemical detection of hydroquinone in wastewater. *New J Chem* 559. <https://doi.org/10.1039/d2nj04285a>
- Wang L, Wang X, Xiao X et al (2013) Reduced graphene oxide/nickel cobaltite nanoflake composites for high specific capacitance supercapacitors. *Electrochim Acta* 111:937–945. <https://doi.org/10.1016/j.electacta.2013.08.094>
- Xu L, Yan P, Li H et al (2017) Photoelectrochemical sensing of bisphenol A based on graphitic carbon nitride/bismuth oxyiodine composites. *RSC Adv* 7:7929–7935. <https://doi.org/10.1039/c6ra25525f>
- Yahya R, Shah A, Kokab T et al (2022) Electrochemical Sensor for Detection and Degradation Studies of Ethyl Violet Dye. *ACS Omega* 7:34154–34165. <https://doi.org/10.1021/acsomega.2c03472>
- Yuan C, Li J, Hou L et al (2012) Facile template-free synthesis of ultralayered mesoporous nickel cobaltite nanowires towards high-performance electrochemical capacitors. *J Mater Chem* 22:16084–16090. <https://doi.org/10.1039/c2jm32351f>

Publisher's note Springer Nature remains neutral with regard to jurisdictional claims in published maps and institutional affiliations.

Springer Nature or its licensor (e.g. a society or other partner) holds exclusive rights to this article under a publishing agreement with the author(s) or other rightsholder(s); author self-archiving of the accepted manuscript version of this article is solely governed by the terms of such publishing agreement and applicable law.